

# Implications of the AMS-02 positron fraction in cosmic rays

Qiang Yuan<sup>a</sup>, Xiao-Jun Bi<sup>a</sup>, Guo-Ming Chen<sup>a</sup>, Yi-Qing Guo<sup>a</sup>, Su-Jie Lin<sup>a</sup>, and Xinmin Zhang<sup>b</sup>

<sup>a</sup>*Key Laboratory of Particle Astrophysics, Institute of High Energy Physics,  
Chinese Academy of Science, Beijing 100049, P.R.China*

<sup>b</sup>*Theoretical Physics Division, Institute of High Energy Physics,  
Chinese Academy of Sciences, Beijing 10049, P.R. China*

(Dated: December 2, 2024)

The AMS-02 collaboration has just released its first result of the cosmic positron fraction  $e^+/(e^- + e^+)$  with high precision up to  $\sim 350$  GeV. The AMS-02 result shows the same trend with the previous PAMELA result, which requires extra electron/positron sources on top of the conventional cosmic ray background, either from astrophysical sources or from dark matter annihilation/decay. In this paper we try to figure out the nature of the extra sources by fitting to the AMS-02  $e^+/(e^- + e^+)$  data, as well as the electron and proton spectra by PAMELA and the  $(e^- + e^+)$  spectrum by Fermi and HESS. We adopt the GALPROP package to calculate the propagation of the Galactic cosmic rays and the Markov Chain Monte Carlo sampler to do the fit. We find that the AMS-02 data have implied essential difference from the PAMELA data. There is tension between the AMS-02  $e^+/(e^- + e^+)$  data and the Fermi/HESS  $(e^- + e^+)$  spectrum, that the AMS-02 data requires less contribution from the extra sources than Fermi/HESS. Then we redo the fit without including the Fermi/HESS data. In this case both the pulsars and dark matter annihilation/decay can explain the AMS-02 data. The pulsar scenario has a soft inject spectrum with the power-law index at  $\sim 2$ , while the dark matter scenario needs  $\tau^+\tau^-$  final state with mass  $\sim 600$  GeV and a boost factor  $\sim 200$ .

PACS numbers: 95.35.+d, 96.50.S-

## I. INTRODUCTION

The Alpha Magnetic Spectrometer (AMS-02) was launched in May 2011. After nearly two years operation and analysis, the AMS-02 collaboration has released its first physical result, i.e. the positron fraction  $e^+/(e^- + e^+)$  in cosmic rays (CRs) [1]. The data show very high precision with the energy range from  $\sim 0.5$  GeV to  $\sim 350$  GeV. The fraction rises above  $\sim 8$  GeV up to the energy end at  $\sim 350$  GeV, which is consistent with the previous PAMELA result of the cosmic positron fraction [2, 3]. The result is NOT consistent with the conventional CR expectation [4]. A great number of works have dedicated to explaining the PAMELA result, either by astrophysical sources [5–10] or by dark matter (DM) [11–15].

To determine the parameters of the CR background and the nature of the extra sources we have to consider all the relevant results. The available results at present include the pure electron spectrum measured by PAMELA [16] and the antiproton flux and ratio  $\bar{p}/p$  [17, 18] by PAMELA. Another important result from PAMELA is the precise measurement of the proton spectrum [19], which determines the secondary positron spectrum by collision with the interstellar medium (ISM) when propagating in the Galaxy. There are also precise measurements of the total electron and positron  $(e^- + e^+)$  spectrum, by the Fermi-LAT collaboration [20, 21] and ATIC collaboration [22]. The ground-based atmospheric Cerenkov telescopes HESS also gives measurement of the total  $e^\pm$  spectrum up to higher energies [23, 24].

Fitting to the PAMELA positron fraction data [2], PAMELA electron spectrum and Fermi/HESS total  $e^\pm$

spectrum shows that both the astrophysical source, such as pulsars, and the DM scenarios can give a good explanation to the data [4]. It is hard to discriminate the two scenarios with the CR spectra mentioned above. As the AMS-02 data show much higher precision and wider energy extension, especially it shows softer behavior than the PAMELA 2008 result, it is necessary to re-examine the previous conclusion with all of the newly available data. In this work we have done such a global fitting to all the relevant data, including AMS-02  $e^+/(e^- + e^+)$ , Fermi and HESS  $(e^- + e^+)$  total spectrum and PAMELA proton and electron spectra.

We adopt the CosRayMC code, which embeds the CR propagation code in the Markov Chain Monte Carlo (MCMC) sampler and enables efficient survey of the high-dimensional parameter space [4, 25]. The CR propagation is treated by the GALPROP package [26]. The CR transportation process in the Galaxy is characterized by the secondary particles. Therefore the secondary-to-primary ratio, such as B/C, (Sc+Ti+V)/Fe, and the unstable-to-stable ratio of secondary particles, such as  $^{10}\text{Be}/^9\text{Be}$ ,  $^{26}\text{Al}/^{27}\text{Al}$  are often used to determine the propagation parameters [26–29]. In this work we fix the CR propagation parameters to the values which give the best fitting to the currently available B/C and  $^{10}\text{Be}/^9\text{Be}$  data with the MCMC method. The fitting process will be reported separately in [30].

We then fit the parameters of the electrons and positrons to the relevant data, both from the CR background and the extra sources. In the work we have considered the continuously distributed pulsars and DM annihilation/decay as two typical scenarios of the extra positron/electron sources. The injection parameters of

primary electrons are free parameters to be fitted. The cosmic positrons include secondaries from CR interaction with the ISM and the primary ones from the extra sources. The secondary positron spectrum is determined by the spectrum of cosmic protons (including Helium and a few heavier nuclei) and the primary positron spectrum is determined by the nature of the extra sources. In principle the injection parameters of the protons can be fitted independently and then be employed to calculate the secondary positrons. However, since both the proton and electron spectra are measured by PAMELA at almost the same time, they are modulated by the solar activity with a similar magnitude. Therefore, in this work we have adopted two ways to fit the cosmic proton injection parameters: either by fitting the proton spectrum independently or by fitting the proton and electron spectra simultaneously. In the first case we enable the protons and electrons/positrons to have different solar modulation parameters, while in the second case we assume they share the same modulation parameter.

By the global fitting we find it seems not easy to fit all the relevant data simultaneously. The AMS-02 data and the Fermi/HESS data might have a *tension* between each other. The AMS-02 requires less contribution from the extra source while Fermi data requires more. We then do the fit without including the Fermi/HESS data. We find in such case both the pulsar and DM scenarios can give good description to the data.

This paper is organized as follows. We give a brief introduction of the propagation of Galactic CRs in Sec. II. The experimental data and fitting method are described in Sec. III. The results are presented in Sec. IV. In Sec. V we give discussion about the fitting results, and finally a brief summary is given in Sec. VI.

## II. COSMIC RAY PROPAGATION

The propagation of charged CRs in the Galaxy is described by the diffusive equation [31]

$$\begin{aligned} \frac{\partial \psi}{\partial t} = & Q(\mathbf{x}, p) + \nabla \cdot (D_{xx} \nabla \psi - \mathbf{V}_c \psi) + \frac{\partial}{\partial p} p^2 D_{pp} \frac{\partial}{\partial p} \frac{1}{p^2} \psi \\ & - \frac{\partial}{\partial p} \left[ \dot{p} \psi - \frac{p}{3} (\nabla \cdot \mathbf{V}_c \psi) \right] - \frac{\psi}{\tau_f} - \frac{\psi}{\tau_r}, \end{aligned} \quad (1)$$

where  $\psi$  is the density of CR particles per unit momentum interval,  $Q(\mathbf{x}, p)$  is the source term,  $D_{xx}$  is the spatial diffusion coefficient,  $\mathbf{V}_c$  is the convection velocity,  $D_{pp}$  is the diffusion coefficient in momentum space used to describe the reacceleration process,  $\dot{p} \equiv dp/dt$  is the momentum loss rate,  $\tau_f$  and  $\tau_r$  are time scales for fragmentation and radioactive decay respectively.  $D_{xx}$  is usually assumed to be only rigidity dependent and has a power-law form  $D_{xx} = D_0 \beta (R/R_0)^\delta$ , with  $\delta$  reflecting the property of the interstellar medium (ISM) turbulence. The reacceleration is described by the diffusion in momentum space. The momentum diffusion coefficient  $D_{pp}$  relates

with the spatial diffusion coefficient  $D_{xx}$  as [32]

$$D_{pp} D_{xx} = \frac{4p^2 v_A^2}{3\delta(4 - \delta^2)(4 - \delta)w}, \quad (2)$$

where  $v_A$  is the Alfvén speed,  $w$  is the ratio of magnetohydrodynamic wave energy density to the magnetic field energy density, which characterizes the level of turbulence. In the usual way we take  $w$  to be 1 and use the Alfvén speed  $v_A$  to describe the reacceleration [32]. The CRs propagate in an extended halo with characteristic height  $z_h$ , beyond which free escape of CRs is assumed. Thus the major propagation parameters include  $D_0$ ,  $\delta$ ,  $v_A$ ,  $V_c$  and  $z_h$ .

There are publicly available numerical codes to compute the CRs propagation in the Galaxy, such as GALPROP<sup>1</sup> [26] and DRAGON<sup>2</sup> [33]. We have embedded the GALPROP package with the MCMC sampler and fitted to the data to constrain the propagation parameters [30].

Recently several groups employed the MCMC technique to fit the CR propagation parameters [34–36]. Using the currently available data of B/C and <sup>10</sup>Be/<sup>9</sup>Be, we did an independent MCMC fit to the propagation parameters [30]. We find the reacceleration model gives quite good description to the present data, while the convection model gives worse fitting. Therefore we adopt the reacceleration (i.e.,  $V_c = 0$ ) scenario as the starting point of the present study. The values of the propagation parameters we adopted in the work are listed in Table I, as given in [30].

TABLE I: Propagation parameters taken in the work

$D_0(10^{28} \text{ cm}^2 \text{ s}^{-1})^a$	5.94
$\delta$	0.377
$z_h(\text{kpc})$	4.04
$v_A(\text{km s}^{-1})$	36.4

<sup>a</sup>At  $R_0 = 4 \text{ GV}$ .

## III. FITTING DESCRIPTION

### A. Model

In the conventional CR model the positrons are secondary particles generated by the interaction between the primary nuclei and the ISM. Wide studies of the PAMELA result show that, besides the secondary positrons, extra sources of positron/electron are necessary to explain the positron fraction  $e^+/(e^- + e^+)$  [4]. The present model to fit the AMS-02 data also includes the traditional CR background (primary nuclei

<sup>1</sup> <http://galprop.stanford.edu/>

<sup>2</sup> <http://www.desy.de/~maccione/DRAGON/>

and electrons, and the secondary positrons) and the extra positron/electron sources.

The injection spectra of the primary protons (heavier nuclei are less relevant) and electrons are assumed to be broken power-law functions with respect to the momentum  $p$

$$q(p) \propto \left( \frac{p}{p_{\text{br}}} \right)^{-\nu_1/\nu_2}, \quad (3)$$

where  $\nu_1$  and  $\nu_2$  are the spectral indices below and above the break momentum  $p_{\text{br}}$ . In the following we use  $\nu_1$  and  $\nu_2$  to represent the proton spectrum and use  $\gamma_1$  and  $\gamma_2$  to represent the primary electron spectrum. The propagated fluxes of protons and electrons are then normalized to factors  $A_p$  and  $A_e$  to get the absolute fluxes.

The spatial distribution of the primary CR particles is adopted to be the supernova remnants (SNR) like distribution

$$f(R, z) \propto \left( \frac{R}{R_\odot} \right)^a \exp \left[ -\frac{b(R - R_\odot)}{R_\odot} \right] \exp \left( -\frac{|z|}{z_s} \right), \quad (4)$$

where  $R_\odot = 8.5$  kpc is the distance of solar system from the Galactic center,  $z_s \approx 0.2$  kpc is the characteristic height of the Galactic disk. We employ  $a = 1.25$  and  $b = 3.56$  following [36].

We employ the parameterization given in [37] to calculate the secondary electron/positron spectra from  $pp$  collision. Another free factor  $c_{e+}$  to normalize the secondary positron/electron flux is included in the fitting, which represents the possible uncertainties from the hadronic interactions, propagation models, the ISM density distributions, and the nuclear enhancement factor from heavy elements.

About the extra electron/positron sources, we study two popular kinds of sources: the astrophysical sources such as pulsars and the DM annihilation scenario. The injection spectrum of pulsars is parameterized as a power-law function with an exponential cutoff

$$q(p) = A_{\text{psr}} p^{-\alpha} \exp(-p/p_c), \quad (5)$$

where  $A_{\text{psr}}$  is the normalization factor,  $\alpha$  is the spectral index and  $p_c$  is the cutoff momentum. The pulsar population is taken to be a continuous form with distribution function (4), but with different parameters  $a = 2.35$  and  $b = 5.56$ , given in [38]. The effect of nearby isolate pulsars (e.g., [5–7], see also the discussion in Sec. V) is not covered in the present study.

For the DM annihilation scenario, the density profile of the Milky Way halo is adopted to be the Navarro-Frenk-White (NFW) distribution [39]

$$\rho(r) = \frac{\rho_s}{(r/r_s)(1 + r/r_s)^2}, \quad (6)$$

with  $r_s = 20$  kpc and  $\rho_s = 0.26$  GeV cm $^{-3}$ . Such a value of  $\rho_s$  will correspond to a local density of 0.3 GeV cm $^{-3}$ . For higher values of the local density as revealed

by several recent studies [40–42], the annihilation cross section will be different by a constant factor. Since the measurement of CR antiprotons by PAMELA [17, 18] constrain the hadronic annihilation channels strongly [11, 12, 43, 44], we will focus on the leptonic annihilation channels here. The positron spectrum from the DM annihilation products is calculated using the PYTHIA simulation package [45].

The CRs at low energy (typically with rigidity below  $\sim 30$  GV) are affected by the solar environment when entering the solar system, known as solar modulation effect. The force field approximation is often employed to describe the solar modulation effect [46], which has only one single parameter — the modulation potential  $\phi$ . However, the low energy data about the positron fraction measured by PAMELA and AMS-02 may imply that the simple force field approximation is not enough to explain the data, and the charge-sign dependent modulation effect is necessary [47–49]. Therefore, in order to avoid possible inconsistency of the low energy behavior we do not include the AMS-02 data below 5 GeV in our fit. The solar modulation effect above 5 GeV is negligible [49, 50].

In summary the full parameter space investigated in this work is

$$\mathcal{P} = \begin{cases} \{A_p, \nu_1, \nu_2, p_{\text{br}}^p\}, & \text{bkg protons,} \\ \{A_e, \gamma_1, \gamma_2, p_{\text{br}}^e\}, & \text{bkg electrons,} \\ \{A_{\text{psr}}, \alpha, p_c\} \text{ or } \{m_\chi, \langle\sigma v\rangle\}, & \text{exotic sources,} \\ \{c_{e+}, \phi\}, & \text{others.} \end{cases} \quad (7)$$

## B. Data

In this study the data to be fitted include the latest positron fraction by AMS-02[1], the electron spectrum by PAMELA [16], the total electron and positron spectra by Fermi [20, 21] and HESS [23, 24]. As for the proton spectrum which will affect the secondary positron production, we choose two ways to deal with it as described in Sec. I: to fix it to the PAMELA measurement [19] or to include the injection parameters in the fit.

Note that the CR spectral hardening at  $\sim 200$  GV reported by ATIC [51], CREAM [52] and PAMELA [19] implies that single power-law can not fully describe the high energy spectra of the CR nuclei above  $\sim 10$  GV. Therefore we only take the PAMELA proton data below 150 GeV in the fit. To better fit the high energy part (and the CREAM data), we need a further break or a curved injection spectrum of the protons [53].

Since the Fermi and HESS data may have larger systematic uncertainties we also investigate the case without the Fermi/HESS data. The definition of the fittings are compiled in Table II.

TABLE II: Definition of fitting

I-a	AMS $e^+/e^\pm$ + PAMELA $e^-$ + Fermi/HESS $e^\pm$
II-a	AMS $e^+/e^\pm$ + PAMELA $e^-$
I-b	AMS $e^+/e^\pm$ + PAMELA $e^-$ + Fermi/HESS $e^\pm$ + PAMELA $p$
II-b	AMS $e^+/e^\pm$ + PAMELA $e^-$ + PAMELA $p$

#### IV. RESULTS

##### A. Fixing the proton spectrum

We first fit the proton spectrum independently with the PAMELA (and CREAM) data. Here we add the high energy CREAM data [52] in the fit to give a description of the proton behavior in a wider energy range. The best fitting injection parameters of protons are:  $\nu_1 = 1.79$ ,  $\nu_2 = 2.36$ ,  $p_{\text{br}}^p = 11.7$  GeV and the solar modulation potential  $\phi = 470$  MV. The propagated proton spectrum for the best fitting parameters is shown in Fig. 1.

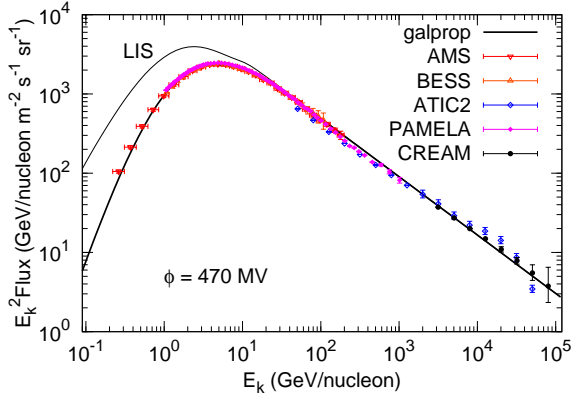


FIG. 1: Proton spectrum derived through fitting PAMELA data. References of the proton data: AMS [54], BESS [55], ATIC2 [51], PAMELA [19] and CREAM [52].

We then run the fits I-a, II-a to derive the parameters of CR electrons/positrons with the best fitting proton spectrum. The resulting positron fraction and electron spectrum for the best fitting parameters of each fit, for both the pulsar and DM scenarios, are shown in Figs. 2 - 4. For each figure, the panels from left to right correspond to the fits I-a and II-a respectively. The best fitting parameters, mean values and their  $1\sigma$  uncertainties are compiled in Tables III - V, and the best fitting  $\chi^2$  over the number of degree of freedom (dof) are given in Table VI.

From Fig. 2 we can see that adding a pulsar component can roughly reproduce the AMS-02 positron fraction data and the Fermi/HESS total electron spectra. However, it also shows a *tension* between the AMS-02 positron fraction and the Fermi/HESS electron spectra, under the current framework. Quantitatively, the best fitting  $\chi^2$  is about 279 for fit I-a. For 151 dof such a  $\chi^2$

means  $\sim 6.1\sigma$  deviation from what expected. The best fitting model is a little over-estimated compared with the AMS-02 data, while under-estimated compared with the Fermi data. This is clearly seen from the fits II-a, in which the constraints of Fermi/HESS data are removed. We see that the fit II-a gives good fit to the AMS-02 data, but deviate from the Fermi data obviously.

Compared with the fitting results with PAMELA positron fraction data [4], the spectrum of the pulsar component becomes much softer (with power-law index  $\sim 1.9$ ), which may be more reasonable according to the pulsar modeling [7]. The contribution of  $e^\pm$  from the pulsars is also smaller than previous estimated according to the PAMELA data. Our fit shows that up to TeV the positron fraction is only  $\sim 20\%$ , while it is more than 30% or even reaching 40% according to the fitting to the PAMELA data.

Figs. 3 and 4 give the results for the DM annihilation scenario. The *tension* between AMS-02 and Fermi/HESS data becomes stronger and the fits get worse than the pulsar scenario. For DM annihilation into  $\mu^+\mu^-$ , the reduced  $\chi^2$  for fit I-a is as high as 3.3. The reason of the poor fit is that the positron spectrum from DM annihilation to a pair of  $\mu^+\mu^-$  is too hard. This can be seen from the top-left panel of Fig. 3. The DM component will over-produce high energy positrons ( $> 100$  GeV) but under-produce positrons at tens of GeV. For fits I-a, heavy DM with mass  $\sim 2-3$  TeV is required due to the constraints of Fermi/HESS data. If we throw away the Fermi/HESS  $e^\pm$  data (fit II-a), we find the AMS-02 data tend to favor lighter DM particles. In this case the 10 - 50 GeV AMS-02 data can be better reproduced, however, the data above 100 GeV are still difficult to be explained.

The situation for  $\tau^+\tau^-$  final state is better. Similar with the  $\mu^+\mu^-$  channel, the positron spectrum from tauon decay is still too hard. Relaxing the constraints from Fermi/HESS data we find a lighter DM mass,  $\sim 550 - 750$  GeV is favored. In this case the AMS-02 data can be fitted relatively well. It is interesting to note that even only the AMS-02 data and PAMELA electron data are considered (fit II-a), the mass of DM particles can be constrained in a small region. Such a strong constraint comes from the very high precise AMS-02 data at lower energy (a few tens GeV). Therefore, we should not take these values too seriously. The change of the background, such as taking different propagation parameters or hadronic interaction models (we will discuss this issue later), may affect the detailed parameters.

Fig. 5 gives the  $1\sigma$  and  $2\sigma$  contour for the DM mass



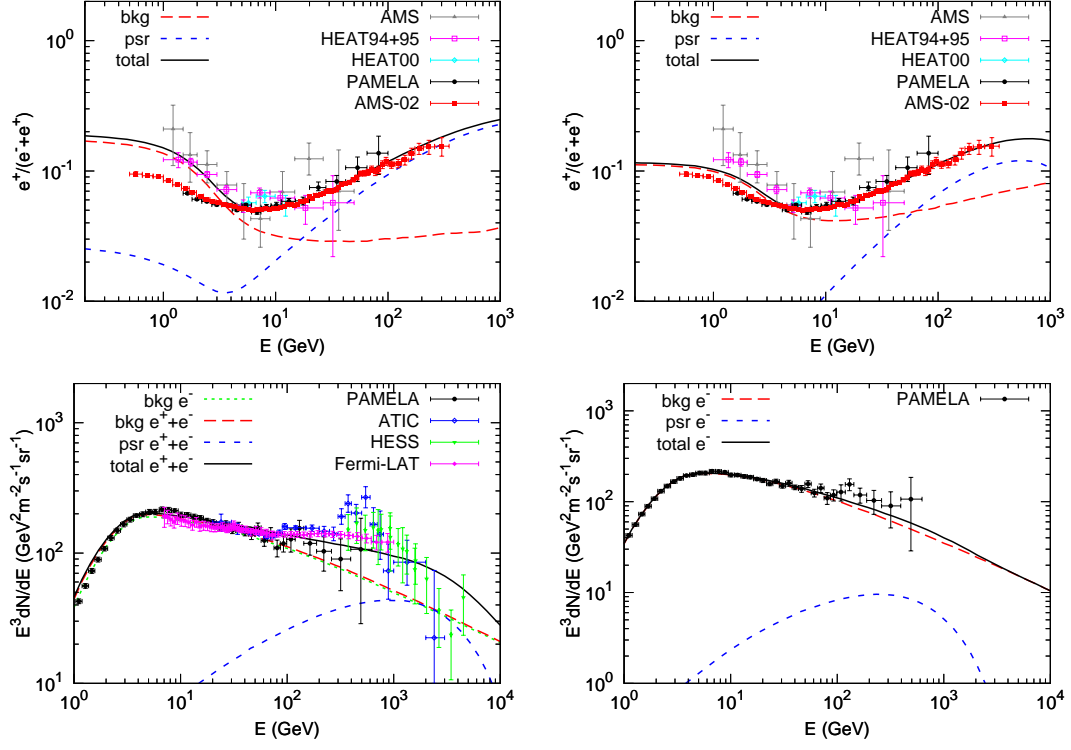


FIG. 2: The positron fraction (upper) and electron spectra (lower) for the background together with a pulsar-like component of the exotic  $e^\pm$ . The panels from left to right are for fits I-a and II-a respectively. References of the data: positron fraction — AMS [56], HEAT94+95 [57], HEAT00 [58], PAMELA [2], AMS-02[1] ; electron — PAMELA [16], ATIC [22], HESS [23, 24], Fermi-LAT [21].

TABLE III: Fitting results of pulsar-like model with proton spectrum fixed

	I-a		II-a	
	best	mean	best	mean
$\log(A_e^a)$	-8.978	$-8.974 \pm 0.005$	-8.925	$-8.921 \pm 0.011$
$\gamma_1$	1.504	$1.512 \pm 0.010$	1.708	$1.704 \pm 0.084$
$\gamma_2$	2.645	$2.652 \pm 0.010$	2.794	$2.796 \pm 0.028$
$\log(p_{\text{br}}^e/\text{MeV})$	3.599	$3.587 \pm 0.022$	3.597	$3.600 \pm 0.046$
$\log(A_{\text{psr}}^b)$	-24.867	$-24.918 \pm 0.146$	-25.257	$-25.226 \pm 0.562$
$\alpha$	1.912	$1.903 \pm 0.029$	1.856	$1.863 \pm 0.116$
$\log(p_c/\text{MeV})$	6.640	$6.632 \pm 0.111$	5.927	$6.097 \pm 0.412$
$c_{e+}$	1.272	$1.327 \pm 0.075$	2.206	$2.222 \pm 0.242$
$\phi/\text{MV}$	500	$527 \pm 30$	818	$830 \pm 72$

<sup>a</sup>Normalization at 25 GeV in unit of  $\text{cm}^{-2}\text{s}^{-1}\text{sr}^{-1}\text{MeV}^{-1}$ .

<sup>b</sup>Normalization at 1 MeV in unit of  $\text{cm}^{-3}\text{s}^{-1}\text{MeV}^{-1}$ .

and annihilation cross section. But we should keep in mind that such results should not be considered statistically meaningful as the fits are quite bad. The solid lines shown in Fig. 5 are the exclusion limits derived by the Fermi  $\gamma$ -ray observations of the Galactic center [59] and dwarf galaxies [60]. We can see that  $\gamma$ -rays tend to give strong constraints on the DM scenario, especially for the  $\tau^+\tau^-$  final state.

We further note that for the DM scenario, the parameter  $\phi$  is very large. The solar modulation potential is assumed to vary between 300 and 1000 MV in these fits. From Tables III - V we see that almost in all cases the modulation potential tends to the upper end. This might be inconsistent with the fact that PAMELA and AMS-02 work approaching the solar minimum.

Since there might be discrepancy between the AMS-

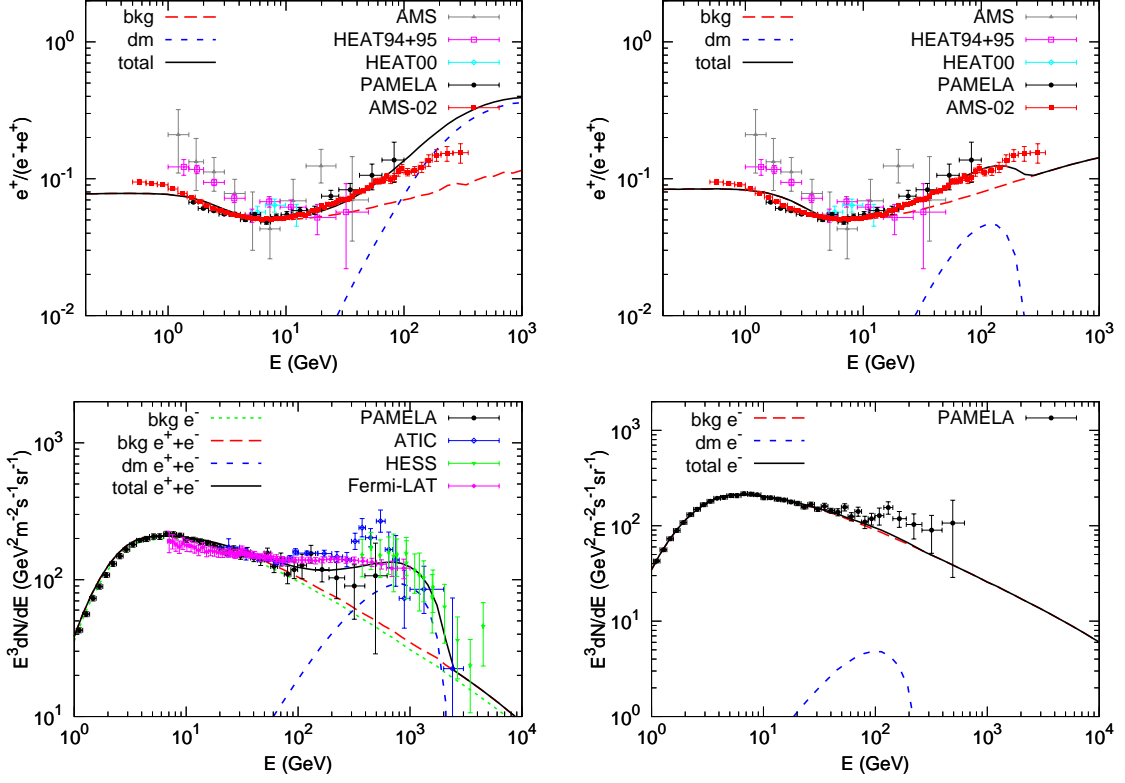


FIG. 3: Same as Fig. 2 but the exotic  $e^\pm$  are assumed to be from DM annihilation. The annihilation channel is  $\mu^+\mu^-$ .

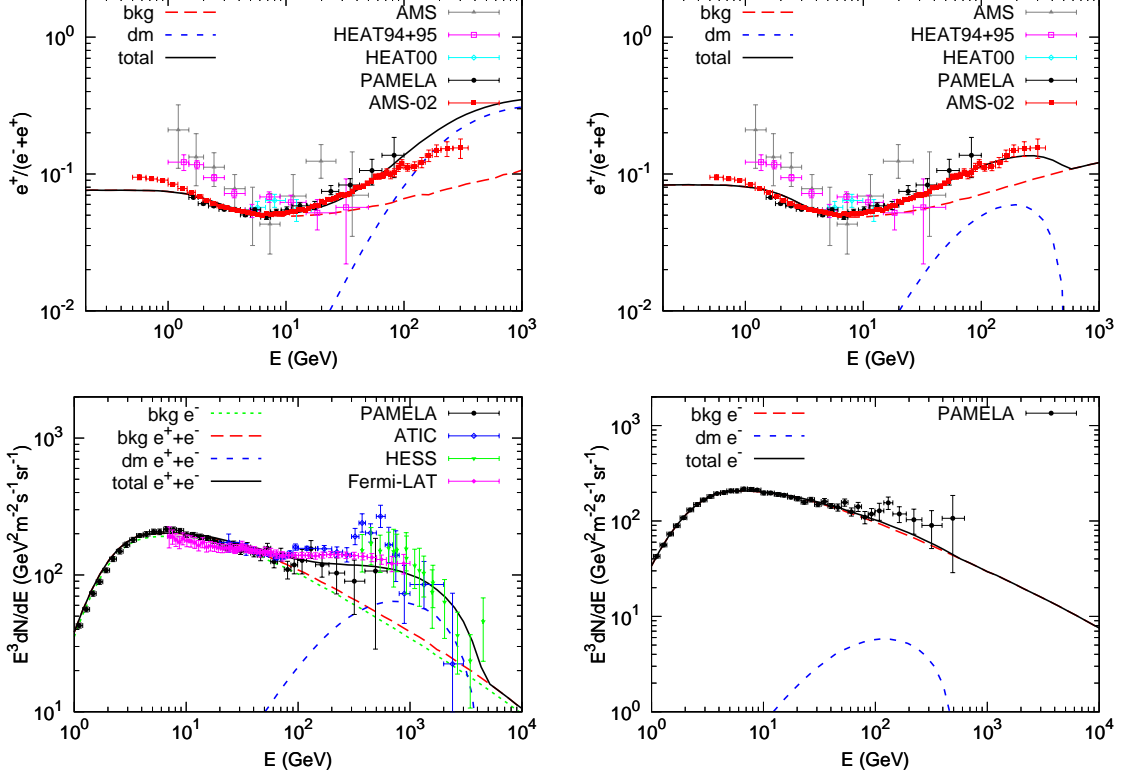


FIG. 4: Same as Fig. 2 but the exotic  $e^\pm$  are assumed to be from DM annihilation. The annihilation channel is  $\tau^+\tau^-$ .

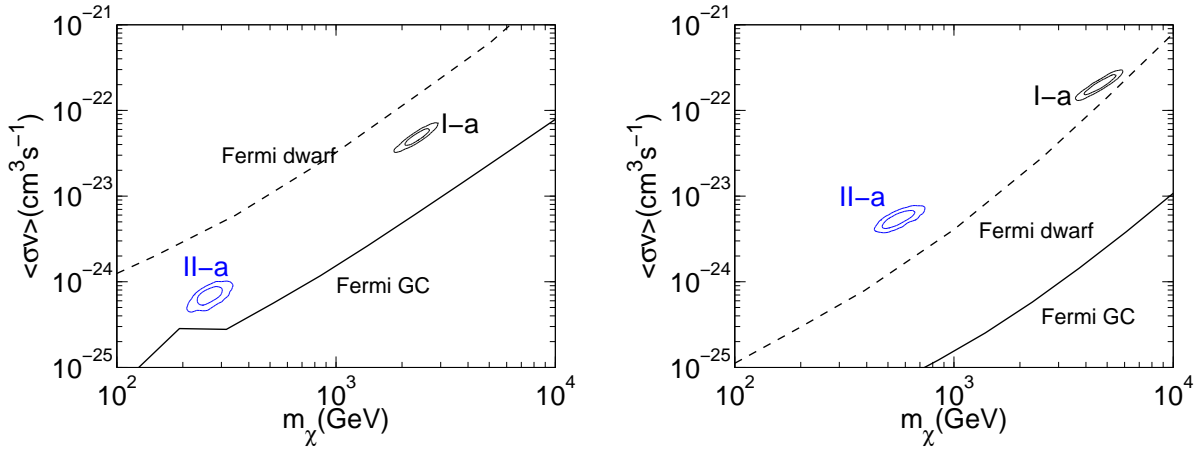
02 and Fermi/HESS data, we give the expected fluxes of pure positrons and electrons separately in Fig. 6 based on

TABLE IV: Fitting results of DM annihilation to  $\mu^+\mu^-$  with proton spectrum fixed

	I-a		II-a	
	best	mean	best	mean
$\log(A_e^a)$	-8.916	$-8.916 \pm 0.003$	-8.915	$-8.918 \pm 0.006$
$\gamma_1$	1.894	$1.870 \pm 0.036$	1.896	$1.868 \pm 0.036$
$\gamma_2$	2.839	$2.839 \pm 0.006$	2.904	$2.906 \pm 0.014$
$\log(p_{\text{br}}^e/\text{MeV})$	3.608	$3.592 \pm 0.035$	3.692	$3.674 \pm 0.037$
$\log(m_\chi/\text{GeV})$	3.371	$3.368 \pm 0.039$	2.415	$2.423 \pm 0.039$
$\log(\langle\sigma v\rangle/\text{cm}^3\text{s}^{-1})$	-22.307	$-22.313 \pm 0.067$	-24.169	$-24.166 \pm 0.069$
$c_{e+}$	2.881	$2.881 \pm 0.030$	3.052	$3.038 \pm 0.047$
$\phi/\text{MV}$	999	$996 \pm 4$	999	$991 \pm 8$

<sup>a</sup>Normalization at 25 GeV in unit of  $\text{cm}^{-2}\text{s}^{-1}\text{sr}^{-1}\text{MeV}^{-1}$ .TABLE V: Fitting results of DM annihilation to  $\tau^+\tau^-$  with proton spectrum fixed

	I-a		II-a	
	best	mean	best	mean
$\log(A_e^a)$	-8.915	$-8.916 \pm 0.003$	-8.907	$-8.909 \pm 0.006$
$\gamma_1$	1.879	$1.878 \pm 0.037$	1.869	$1.817 \pm 0.070$
$\gamma_2$	2.813	$2.813 \pm 0.007$	2.863	$2.856 \pm 0.015$
$\log(p_{\text{br}}^e/\text{MeV})$	3.570	$3.571 \pm 0.037$	3.637	$3.608 \pm 0.058$
$\log(m_\chi/\text{GeV})$	3.667	$3.665 \pm 0.045$	2.765	$2.747 \pm 0.046$
$\log(\langle\sigma v\rangle/\text{cm}^3\text{s}^{-1})$	-21.699	$-21.703 \pm 0.073$	-23.261	$-23.269 \pm 0.064$
$c_{e+}$	2.773	$2.769 \pm 0.035$	2.900	$2.844 \pm 0.068$
$\phi/\text{MV}$	999	$994 \pm 5$	998	$974 \pm 20$

<sup>a</sup>Normalization at 25 GeV in unit of  $\text{cm}^{-2}\text{s}^{-1}\text{sr}^{-1}\text{MeV}^{-1}$ .FIG. 5:  $1\sigma$  and  $2\sigma$  confidence regions on the DM mass and cross section plane, for the fits I-a and II-a respectively. The left panel is for  $\mu^+\mu^-$  channel, and the right panel is for  $\tau^+\tau^-$  channel. The solid lines show the 95% upper limit of Fermi  $\gamma$ -ray observations of the Galactic center (with normalization of the local density corrected) [59] and dwarf galaxies [60].

the fit II-a (i.e., without Fermi/HESS data). It is shown that the electron spectrum shows an almost featureless behavior and the extra component is difficult to be identified from the pure electron spectrum. It is more prominent to see the extra component in the positron spec-

trum, which has a very hard spectrum ( $\sim E^{-2.8}$ ) above  $\sim 10$  GeV. The following measurement of the positron and electron fluxes by AMS-02 can directly test such results.

TABLE VI: Summary of fitting  $\chi^2/\text{dof}$ . Note that the AMS-02 data above 5 GeV and PAMELA proton data below 150 GeV are used to calculate the  $\chi^2$ .

	pulsar	DM ( $\mu^+\mu^-$ )	DM ( $\tau^+\tau^-$ )
I-a	278.7/151	506.7/152	496.5/152
II-a	51.5/80	83.1/81	56.7/81
I-b	288.0/205	615.3/206	584.6/206
II-b	83.0/134	238.7/135	164.3/135

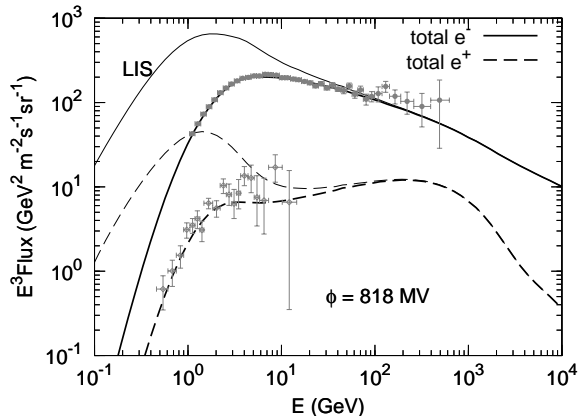


FIG. 6: Expected fluxes of electrons (solid) and positrons (dashed) for the fit II-a. The higher one in each group is the local interstellar (LIS) flux and the lower one represents the flux after the solar modulation. Grey points show the PAMELA measurement of electrons [16] and CAPRICE measurement of positrons [61].

## B. Relaxing the proton spectrum

Since the proton spectrum will affect the secondary positron production, and also the determination of the solar modulation parameter, we take the proton spectrum into account and redo the fits (labeled as I-b and II-b). The fitting results with the best fitting parameters are presented in Figs. 7-9. The best fitting results, mean values and the  $1\sigma$  uncertainties of the model parameters are listed in Tables VII-IX, and the best fitting  $\chi^2$  over dof are also presented in Table VI. Qualitatively we find that the results are similar with that in the previous subsection.

For the pulsar scenario, the minimum  $\chi^2$  for fit I-b is about 288, which corresponds to a  $\sim 3.9\sigma$  deviation from what expected for 205 dof. Compared with the fits of fixed proton spectrum, the injection spectrum of positrons from pulsars is a little bit softer here. This is because the proton spectrum here is also softer than that in the previous subsection. Therefore a softer pulsar-induced positron spectrum is required to give more tens of GeV positrons and to compensate the effect of a softer proton spectrum.

The DM scenario fits worse than the pulsar scenario. As we have discussed, the reason is that the DM-induced

positron spectrum is too hard. The  $1\sigma$  and  $2\sigma$  confidence level contours on the  $m_\chi - \langle\sigma v\rangle$  plane for the fits are shown in Fig. 10. The parameter regions differ only slightly from that derived in the previous subsection (Fig. 5). The strong constraints on the DM model from  $\gamma$ -rays are not changed.

From Figs. 8 and 9 we note that the proton spectrum can not be well fitted for the DM scenario. This is also due to the hard positron spectrum from DM annihilation into muons and taus. A harder proton spectrum will produce more positrons above  $\sim 10$  GeV, which will compensate the lack of positrons from the hard spectrum of the DM component. If we reduce the constraints from Fermi/HESS data (fits II-b), we see that the proton spectrum fits the data better.

We also note from Figs. 8 and 9 that when not including Fermi/HESS data the DM scenario does not give a good description to the high energy end of the AMS-02 data, which is different from the pulsar case shown in Fig. 7. This is because the positron spectrum is determined once the mass of DM and its annihilation final states are given. To have a minimum  $\chi^2$  the mass of DM (i.e. the shape of the positron spectrum) is usually determined by the data at tens of GeV where the errors are very small, instead of the behavior of the high energy end data.

The solar modulation potential  $\phi$  and  $c_{e^+}$  at the DM case are larger than that in the pulsar case. The reason is that the DM spectrum is always harder than the pulsar case. To fit the AMS-02 data at tens of GeV, which are very precise, larger  $\phi$  and  $c_{e^+}$  can give relatively higher flux of positrons in this energy range.

## C. Further tests

To better understand how soft a positron spectrum from the extra sources is needed, we show in Fig. 11 the  $2\sigma$  range of source spectra from pulsars at the solar location with shaded regions. The  $2\sigma$  range is defined with  $\Delta\chi^2 = \chi^2 - \chi^2_{\min} = 22.7$  for 13 fitting parameters. For comparison the DM induced positron spectra for  $\mu^+\mu^-$ ,  $\tau^+\tau^-$ ,  $W^+W^-$  and  $b\bar{b}$  channels are also shown. The mass of DM particle is taken to be  $m_\chi = 1$  TeV and a free flux normalization is adopted. It is shown that the positron spectra from DM annihilation in the  $\mu^+\mu^-$  and  $\tau^+\tau^-$  channels are much harder than the pulsar component. For the  $W^+W^-$  and  $b\bar{b}$  channels the spectrum is softer and we would expect a better fit to the data.

As a test we run the fit II-a with DM annihilation to  $W^+W^-$  and  $b\bar{b}$  final states. We find the  $\chi^2$  values become slightly smaller ( $\sim 52.7$  for both  $W^+W^-$  and  $b\bar{b}$ ) than that of  $\tau^+\tau^-$ . The positron fraction and electron spectrum for the best fitting parameters are shown in Fig. 12. It is shown that the AMS-02 positron fraction data can be reproduced in this case.

We know that the PAMELA antiproton data and Fermi  $\gamma$ -ray data set very stringent constraints on the DM annihilation into quark and gauge boson final



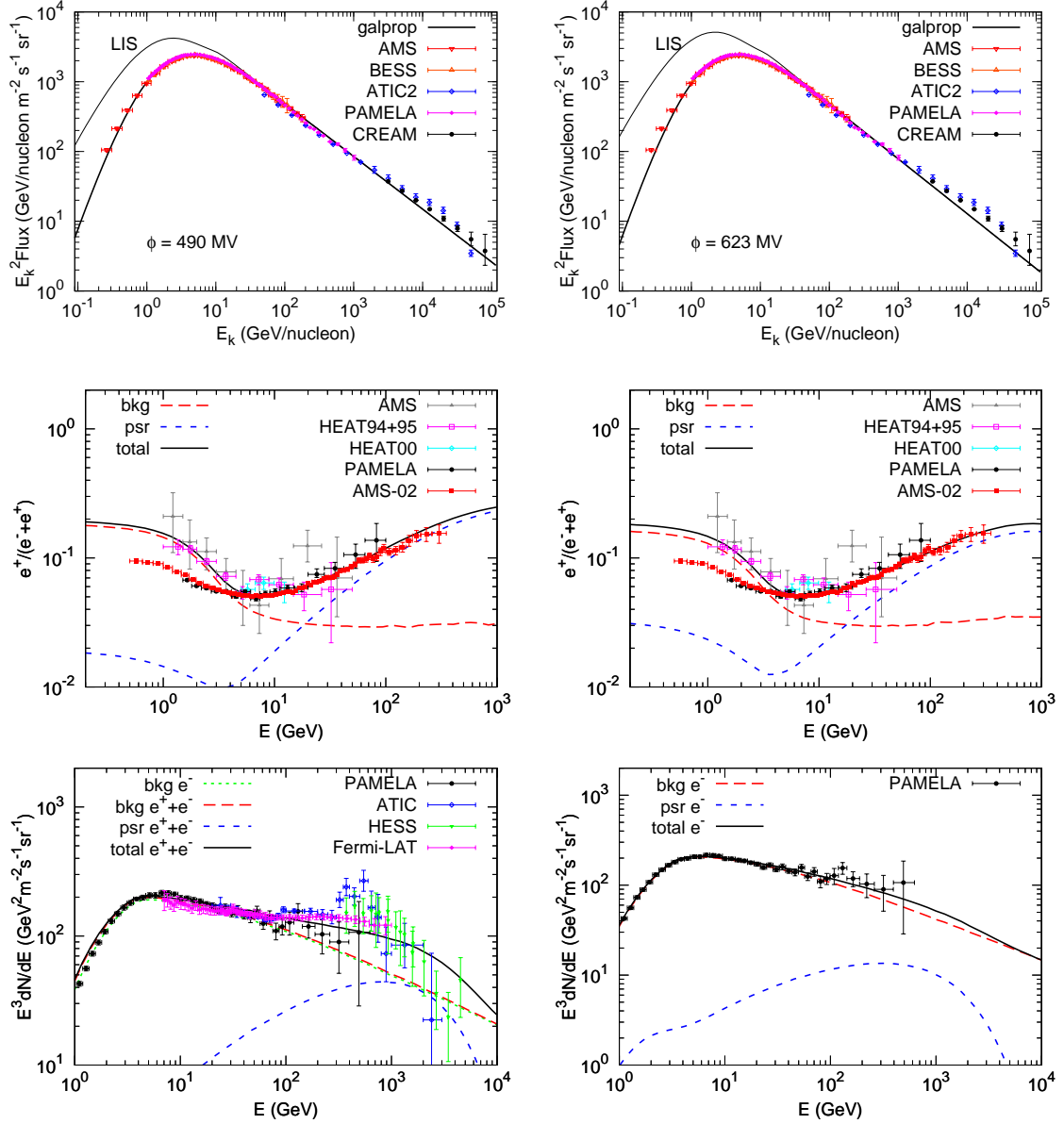


FIG. 7: From top to bottom: the proton, positron fraction and electron spectra for the background together with a pulsar-like component of the exotic  $e^\pm$ . The left and right panels are for fits I-b and II-b respectively.

states[43, 44, 62, 63]. Fig. 13 shows the two dimensional contours on the  $m_\chi - \langle\sigma v\rangle$  plane for the  $W^+W^-$  and  $b\bar{b}$  channels and the 95% exclusion limits on DM annihilation to  $b\bar{b}$  and  $W^+W^-$  channels by Fermi observation of dwarf galaxies [60]. We see that the current positron fraction data of AMS-02, together with other  $e^\pm$ , antiproton and  $\gamma$ -ray data, give strong constraints on the present DM scenario to explain the  $e^\pm$  excesses.

## V. DISCUSSION

### A. Uncertainties of the theoretical model

Since the AMS-02 data are very precise, any uncertainties previously thought to be not important may affect the fitting result. As we note above the positron spectrum around tens of GeV may affect the fitting result sensitively. Therefore the change of the shape of background may affect the fitting results. There are quite a few sources of such uncertainties, such as the propagation parameters, the hadronic interaction models, and so on.

In this work we use the Kamae et al. (2006) parame-

TABLE VII: Fitting results of pulsar-like model with proton spectrum relaxed

	I-b		II-b	
	best	mean	best	mean
$\log(A_p^a)$	-8.323	$-8.327 \pm 0.005$	-8.328	$-8.330 \pm 0.006$
$\nu_1$	1.789	$1.797 \pm 0.019$	1.882	$1.885 \pm 0.023$
$\nu_2$	2.378	$2.388 \pm 0.011$	2.410	$2.415 \pm 0.019$
$\log(p_{\text{br}}^p/\text{MeV})$	4.040	$4.064 \pm 0.029$	4.099	$4.121 \pm 0.031$
$\log(A_e^b)$	-8.977	$-8.979 \pm 0.004$	-8.941	$-8.948 \pm 0.008$
$\gamma_1$	1.504	$1.505 \pm 0.004$	1.535	$1.554 \pm 0.040$
$\gamma_2$	2.647	$2.645 \pm 0.011$	2.720	$2.722 \pm 0.018$
$\log(p_{\text{br}}^e/\text{MeV})$	3.615	$3.614 \pm 0.015$	3.614	$3.631 \pm 0.016$
$\log(A_{\text{psr}}^c)$	-25.104	$-25.012 \pm 0.132$	-24.494	$-24.411 \pm 0.335$
$\alpha$	1.864	$1.881 \pm 0.026$	1.985	$2.006 \pm 0.068$
$\log(p_c/\text{MeV})$	6.512	$6.562 \pm 0.093$	6.205	$6.442 \pm 0.285$
$c_{e+}$	1.306	$1.276 \pm 0.062$	1.503	$1.468 \pm 0.127$
$\phi/\text{MV}$	490	$489 \pm 21$	623	$614 \pm 37$

<sup>a</sup>Normalization at 100 GeV in unit of  $\text{cm}^{-2}\text{s}^{-1}\text{sr}^{-1}\text{MeV}^{-1}$ .<sup>b</sup>Normalization at 25 GeV in unit of  $\text{cm}^{-2}\text{s}^{-1}\text{sr}^{-1}\text{MeV}^{-1}$ .<sup>c</sup>Normalization at 1 MeV in unit of  $\text{cm}^{-3}\text{s}^{-1}\text{MeV}^{-1}$ .TABLE VIII: Fitting results of DM annihilation into  $\mu^+\mu^-$  with proton spectrum relaxed

	I-b		II-b	
	best	mean	best	mean
$\log(A_p^a)$	-8.275	$-8.276 \pm 0.004$	-8.299	$-8.298 \pm 0.004$
$\nu_1$	1.936	$1.947 \pm 0.031$	2.037	$2.026 \pm 0.022$
$\nu_2$	2.271	$2.281 \pm 0.009$	2.364	$2.365 \pm 0.010$
$\log(p_{\text{br}}^p/\text{MeV})$	3.919	$3.929 \pm 0.045$	4.102	$4.101 \pm 0.035$
$\log(A_e^b)$	-8.953	$-8.950 \pm 0.006$	-8.938	$-8.944 \pm 0.008$
$\gamma_1$	1.555	$1.588 \pm 0.054$	1.789	$1.754 \pm 0.046$
$\gamma_2$	2.768	$2.773 \pm 0.011$	2.890	$2.895 \pm 0.016$
$\log(p_{\text{br}}^e/\text{MeV})$	3.578	$3.573 \pm 0.027$	3.679	$3.670 \pm 0.026$
$\log(m_\chi/\text{GeV})$	3.330	$3.338 \pm 0.045$	2.390	$2.417 \pm 0.038$
$\log(\langle\sigma v\rangle/\text{cm}^3\text{s}^{-1})$	-22.397	$-22.381 \pm 0.076$	-24.142	$-24.117 \pm 0.060$
$c_{e+}$	1.996	$2.037 \pm 0.064$	2.541	$2.527 \pm 0.070$
$\phi/\text{MV}$	702	$729 \pm 39$	879	$866 \pm 36$

<sup>a</sup>Normalization at 100 GeV in unit of  $\text{cm}^{-2}\text{s}^{-1}\text{sr}^{-1}\text{MeV}^{-1}$ .<sup>b</sup>Normalization at 25 GeV in unit of  $\text{cm}^{-2}\text{s}^{-1}\text{sr}^{-1}\text{MeV}^{-1}$ .

terization of the  $pp$  collision [37]. As shown in [64] there were remarkable differences between different hadronic models. The Kamae et al. (2006) parameterization included more processes than before and was calibrated with recent data [37]. However, it depends strongly on the Monte Carlo simulations. Therefore we also test the fitting with old  $pp$  collision parameterization [65]. The results show quantitative difference from that shown above. But, all the conclusions made in the previous section keep unchanged.

### B. Additional spectral break of the primary electrons

As revealed by ATIC, CREAM and PAMELA measurements, the nuclei spectra have a hardening above  $\sim 200$  GV [19, 51, 52]. It is possible that the primary electron spectrum also has a similar hardening at high energies [66]. By including such a modification of the primary electron spectrum may soften the tension between the AMS-02 and Fermi data. This will be investigated in future works.

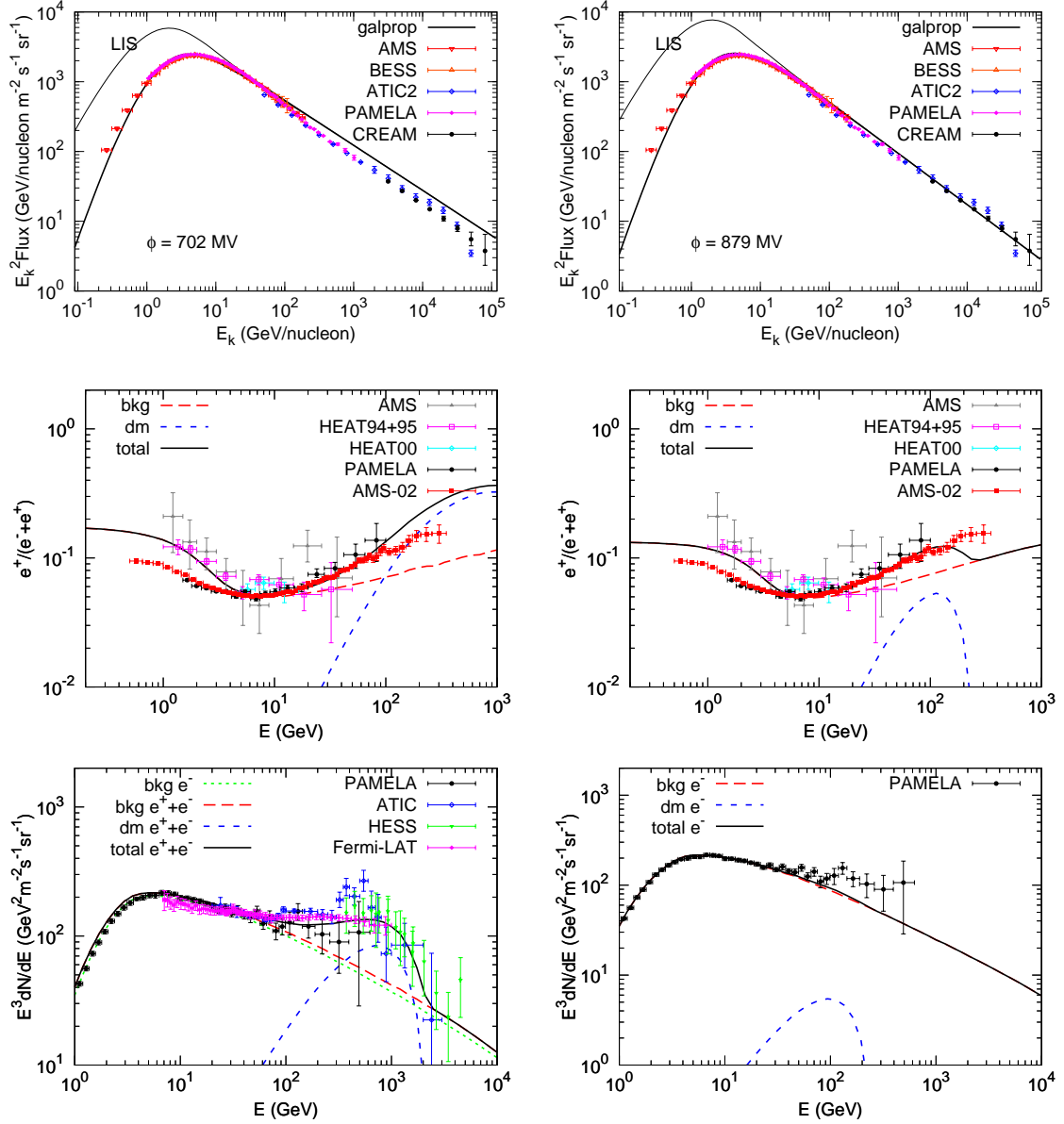


FIG. 8: Same as Fig. 7 but the exotic  $e^\pm$  are assumed to be from DM annihilation. The annihilation channel is  $\mu^+\mu^-$ .

### C. Two or more components of the extra $e^\pm$ sources

It is possible that there are more than one components of the primary sources of positrons. For example for the pulsar scenario, the far away pulsar population may contribute to a “background” component, and several nearby pulsars may give very distinct contributions to the positron spectrum [5]. Such a picture may also help to eliminate the *tension* between AMS-02 data and Fermi/HESS  $e^\pm$  data. The “background” pulsars may give most contributions to the AMS-02 positron excesses, while the nearby sources can contribute mainly at high energies to reproduce the Fermi/HESS data. We leave the detailed modeling in future works.

### D. To improve the DM scenario

Finally we discuss the possibilities to improve the DM scenario to give better explanation of the current data. First we need softer and broader spectrum of positrons from DM. Therefore if the annihilation final state is not two-body state but four-body, eight-body etc., softer positron spectrum may be generated. A mixture of leptonic channels and hadronic channels may also give a broader spectrum (see Fig. 11). Second we have to consider how to avoid the constraints from  $\gamma$ -rays and antiprotons. Decaying DM scenario is better since the constraints from  $\gamma$ -rays are less stringent [67, 68]. As for the antiproton constraints, very massive DM particle may avoid the current bounds set by the PAMELA data

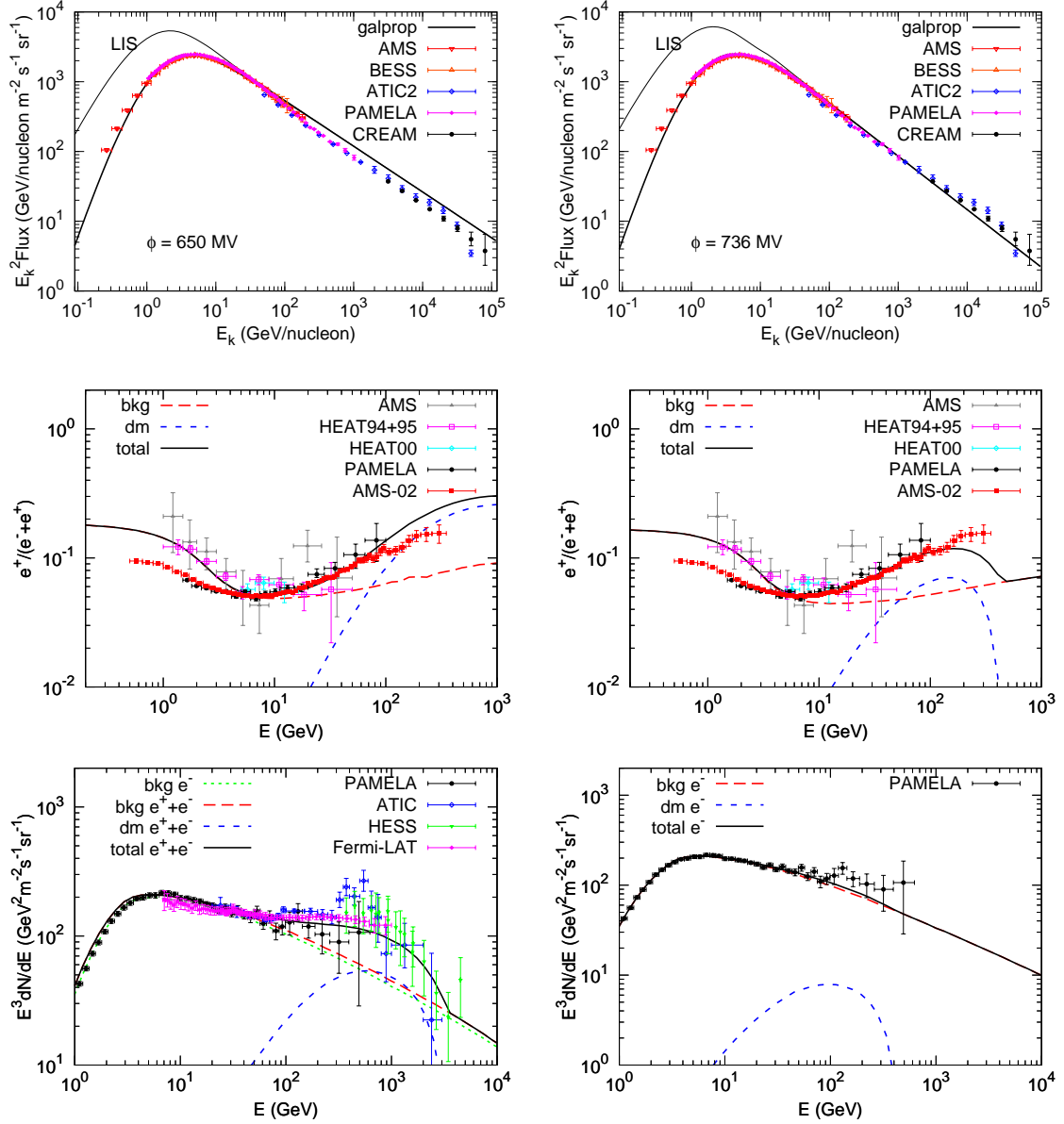


FIG. 9: Same as Fig. 7 but the exotic  $e^\pm$  are assumed to be from DM annihilation. The annihilation channel is  $\tau^+\tau^-$ .

[11].

## VI. SUMMARY

In summary in this work we give a systematical investigation of the models to explain the cosmic  $e^\pm$  excesses, based on the newest AMS-02 data of the positron fraction and other data from PAMELA, Fermi and HESS. Both the pulsar scenario and DM scenario as the extra primary  $e^\pm$  sources are studied. Our findings are as follows.

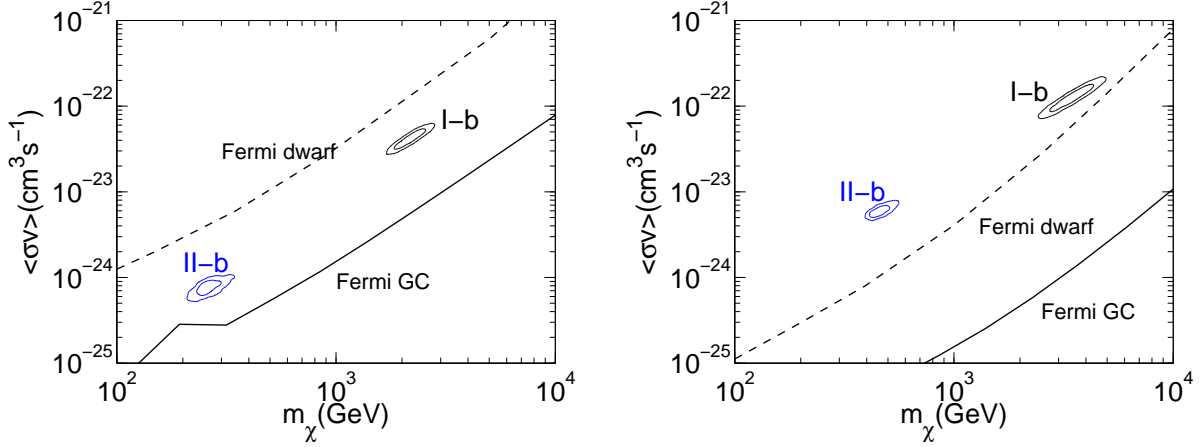
- In the present framework there is *tension* between the AMS-02 data and Fermi/HESS data. The AMS-02 positron fraction data requires less

positrons from the extra sources than that needed by Fermi/HESS data.

- Pulsar models can roughly fit the data. The spectral index of the positrons injected by pulsars is about  $E^{-2}$ , which is much softer than that derived when using the PAMELA positron fraction data.
- If we fit only the AMS-02 positron fraction and PAMELA electron spectrum data both the pulsar and DM annihilates/decays into  $\tau^+\tau^-$ ,  $W^+W^-$  and  $b\bar{b}$  can fit the data.
- Due to the strong constraints from antiprotons and  $\gamma$ -rays, the DM annihilation scenario (into two body final states) seems not easy to be consistent

TABLE IX: Fitting results of DM annihilation into  $\tau^+\tau^-$  with proton spectrum relaxed

	I-b		II-b	
	best	mean	best	mean
$\log(A_p^a)$	-8.278	$-8.282 \pm 0.004$	-8.310	$-8.310 \pm 0.005$
$\nu_1$	1.900	$1.892 \pm 0.023$	1.962	$1.951 \pm 0.030$
$\nu_2$	2.281	$2.285 \pm 0.008$	2.387	$2.381 \pm 0.012$
$\log(p_{\text{br}}^p/\text{MeV})$	3.936	$3.920 \pm 0.032$	4.136	$4.101 \pm 0.037$
$\log(A_e^b)$	-8.962	$-8.961 \pm 0.004$	-8.940	$-8.944 \pm 0.008$
$\gamma_1$	1.512	$1.534 \pm 0.026$	1.637	$1.604 \pm 0.056$
$\gamma_2$	2.730	$2.731 \pm 0.011$	2.794	$2.792 \pm 0.021$
$\log(p_{\text{br}}^e/\text{MeV})$	3.558	$3.569 \pm 0.020$	3.633	$3.610 \pm 0.027$
$\log(m_\chi/\text{GeV})$	3.555	$3.522 \pm 0.075$	2.657	$2.670 \pm 0.031$
$\log(\langle\sigma v\rangle/\text{cm}^3\text{s}^{-1})$	-21.884	$-21.929 \pm 0.116$	-23.222	$-23.216 \pm 0.048$
$c_{e+}$	1.856	$1.875 \pm 0.051$	2.167	$2.151 \pm 0.094$
$\phi/\text{MV}$	650	$649 \pm 29$	736	$733 \pm 47$

<sup>a</sup>Normalization at 100 GeV in unit of  $\text{cm}^{-2}\text{s}^{-1}\text{sr}^{-1}\text{MeV}^{-1}$ .<sup>b</sup>Normalization at 25 GeV in unit of  $\text{cm}^{-2}\text{s}^{-1}\text{sr}^{-1}\text{MeV}^{-1}$ .FIG. 10:  $1\sigma$  and  $2\sigma$  confidence regions on the DM mass and cross section plane, for the fits I-b and II-b respectively. The left panel is for  $\mu^+\mu^-$  channel, and the right panel is for  $\tau^+\tau^-$  channel. The solid lines show the 95% upper limit of Fermi  $\gamma$ -ray observations of the Galactic center (with normalization of the local density corrected) [59] and dwarf galaxies [60].

with all of the current data.

Our study illustrates the remarkable potential on understanding the physics of the  $e^\pm$  excesses from the very precise measurement done by AMS-02. According to the PAMELA positron fraction data, the pulsar and DM scenarios are almost identical [4]. Given the AMS-02 precise measurement, the differences between different scenarios become to appear. We are looking forward to more data with higher precision from AMS-02 to further shed light on the understanding of the fundamental questions of

both astrophysics and particle physics.

#### Acknowledgments

We would like to thank Chen Hesheng, Hu Hongbo, Li Zuhao, Lü Yüsheng, Tang Zhicheng and Xu Weiwei for helpful discussions. This work is supported in part by National Natural Science Foundation of China under Grant Nos. 11075169, 11135009, 11105155 and 11220101004, and by 973 Program under Grant Nos. 2010CB83300 and 2013CB837000.

[1] M. Aguilar, et al., Physical Review Letters **110**, 141102 (2013).

[2] O. Adriani, et al., Nature **458**, 607 (2009), 0810.4995.



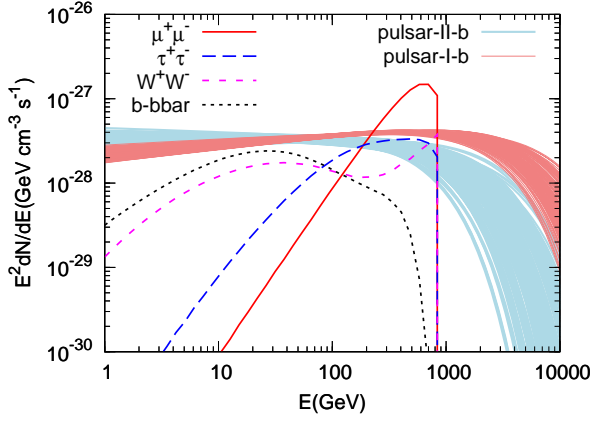


FIG. 11: Shaded regions are 95% intervals of the exotic positron source component at the solar location of pulsar models. The DM-induced positron spectra for  $\mu^+\mu^-$ ,  $\tau^+\tau^-$ ,  $W^+W^-$  and  $b\bar{b}$  channels are shown for comparison.

- [3] O. Adriani, et al., *Astroparticle Physics* **34**, 1 (2010), 1001.3522.
- [4] J. Liu, Q. Yuan, X.-J. Bi, H. Li, and X. Zhang, *Phys. Rev. D* **85**, 043507 (2012), 1106.3882.
- [5] D. Hooper, P. Blasi, and P. Dario Serpico, *J. Cosmol. Astropart. Phys.* **1**, 25 (2009), 0810.1527.
- [6] H. Yüksel, M. D. Kistler, and T. Stanev, *Phys. Rev. Lett.* **103**, 051101 (2009), 0810.2784.
- [7] S. Profumo, *Central European Journal of Physics* **10**, 1 (2012), 0812.4457.
- [8] D. Malyshev, I. Cholis, and J. Gelfand, *Phys. Rev. D* **80**, 063005 (2009), 0903.1310.
- [9] H.-B. Hu, Q. Yuan, B. Wang, C. Fan, J.-L. Zhang, and X.-J. Bi, *Astrophys. J. Lett.* **700**, L170 (2009), 0901.1520.
- [10] P. Blasi, *Phys. Rev. Lett.* **103**, 051104 (2009), 0903.2794.
- [11] M. Cirelli, M. Kadastik, M. Raidal, and A. Strumia, *Nuclear Physics B* **813**, 1 (2009), 0809.2409.
- [12] P. F. Yin, Q. Yuan, J. Liu, J. Zhang, X. J. Bi, S. H. Zhu, and X. M. Zhang, *Phys. Rev. D* **79**, 023512 (2009), 0811.0176.
- [13] L. Bergström, T. Bringmann, and J. Edsjö, *Phys. Rev. D* **78**, 103520 (2008), 0808.3725.
- [14] V. Barger, W.-Y. Keung, D. Marfatia, and G. Shaughnessy, *Phys. Lett. B* **672**, 141 (2009), 0809.0162.
- [15] J. Zhang, X. J. Bi, J. Liu, S. M. Liu, P. F. Yin, Q. Yuan, and S. H. Zhu, *Phys. Rev. D* **80**, 023007 (2009), 0812.0522.
- [16] O. Adriani, et al., *Phys. Rev. Lett.* **106**, 201101 (2011).
- [17] O. Adriani, et al., *Phys. Rev. Lett.* **102**, 051101 (2009), 0810.4994.
- [18] O. Adriani, et al., *Phys. Rev. Lett.* **105**, 121101 (2010), 1007.0821.
- [19] O. Adriani, et al., *Science* **332**, 69 (2011), 1103.4055.
- [20] A. A. Abdo, et al., *Phys. Rev. Lett.* **102**, 181101 (2009), 0905.0025.
- [21] M. Ackermann, et al., *Phys. Rev. D* **82**, 092004 (2010).
- [22] J. Chang, et al., *Nature* **456**, 362 (2008).
- [23] F. Aharonian, et al., *Phys. Rev. Lett.* **101**, 261104 (2008), 0811.3894.
- [24] F. Aharonian, et al., *Astron. Astrophys.* **508**, 561 (2009), 0905.0105.
- [25] J. Liu, Q. Yuan, X. J. Bi, H. Li, and X. M. Zhang, *Phys. Rev. D* **81**, 023516 (2010), 0906.3858.
- [26] A. W. Strong and I. V. Moskalenko, *Astrophys. J.* **509**, 212 (1998), arXiv:astro-ph/9807150.
- [27] T. K. Gaisser, *Cosmic rays and particle physics* (Cambridge and New York, Cambridge University Press, 1990, 292 p., 1990).
- [28] D. Maurin, F. Donato, R. Taillet, and P. Salati, *Astrophys. J.* **555**, 585 (2001).
- [29] G. di Bernardo, C. Evoli, D. Gaggero, D. Grasso, and L. Maccione, *Astroparticle Physics* **34**, 274 (2010), 0909.4548.
- [30] S. J. Lin, C. F. Cai, and et al., in preparation (2013).
- [31] A. W. Strong, I. V. Moskalenko, and V. S. Ptuskin, *Annual Review of Nuclear and Particle Science* **57**, 285 (2007), arXiv:astro-ph/0701517.
- [32] E. S. Seo and V. S. Ptuskin, *Astrophys. J.* **431**, 705 (1994).
- [33] C. Evoli, D. Gaggero, D. Grasso, and L. Maccione, *J. Cosmol. Astropart. Phys.* **10**, 18 (2008), 0807.4730.
- [34] A. Putze, L. Derome, D. Maurin, L. Perotto, and R. Taillet, *Astron. Astrophys.* **497**, 991 (2009), 0808.2437.
- [35] A. Putze, L. Derome, and D. Maurin, *Astron. Astrophys.* **516**, A66 (2010), 1001.0551.
- [36] R. Trotta, G. Jóhannesson, I. V. Moskalenko, T. A. Porter, R. Ruiz de Austri, and A. W. Strong, *Astrophys. J.* **729**, 106 (2011), 1011.0037.
- [37] T. Kamae, N. Karlsson, T. Mizuno, T. Abe, and T. Koi, *Astrophys. J.* **647**, 692 (2006), arXiv:astro-ph/0605581.
- [38] D. R. Lorimer, in *Young Neutron Stars and Their Environments*, edited by F. Camilo & B. M. Gaensler (2004), vol. 218 of *IAU Symposium*, p. 105.
- [39] J. F. Navarro, C. S. Frenk, and S. D. M. White, *Astrophys. J.* **490**, 493 (1997), arXiv:astro-ph/9611107.
- [40] R. Catena and P. Ullio, *J. Cosmol. Astropart. Phys.* **8**, 4 (2010), 0907.0018.
- [41] P. Salucci, F. Nesti, G. Gentile, and C. Frigerio Martins, *Astron. Astrophys.* **523**, A83 (2010), 1003.3101.
- [42] M. Pato, O. Agertz, G. Bertone, B. Moore, and R. Teyssier, *Phys. Rev. D* **82**, 023531 (2010), 1006.1322.
- [43] F. Donato, D. Maurin, P. Brun, T. Delahaye, and P. Salati, *Phys. Rev. Lett.* **102**, 071301 (2009), 0810.5292.
- [44] I. Cholis, *J. Cosmol. Astropart. Phys.* **9**, 007 (2011), 1007.1169.
- [45] T. Sjöstrand, S. Mrenna, and P. Skands, *Journal of High Energy Physics* **5**, 26 (2006), arXiv:hep-ph/0603175.
- [46] L. J. Gleeson and W. I. Axford, *Astrophys. J.* **154**, 1011 (1968).
- [47] J. M. Clem, D. P. Clements, J. Esposito, P. Evenson, D. Huber, J. L'Heureux, P. Meyer, and C. Constantin, *Astrophys. J.* **464**, 507 (1996).
- [48] B. Beischer, P. von Doetinchem, H. Gast, T. Kirn, and S. Schael, *New Journal of Physics* **11**, 105021 (2009).
- [49] S. Della Torre, et al., *Advances in Space Research* **49**, 1587 (2012).
- [50] L. Maccione, *Physical Review Letters* **110**, 081101 (2013), 1211.6905.
- [51] A. D. Panov, et al., *Bulletin of the Russian Academy of Science, Phys.* **71**, 494 (2007), arXiv:astro-ph/0612377.
- [52] H. S. Ahn, et al., *Astrophys. J. Lett.* **714**, L89 (2010), 1004.1123.
- [53] Q. Yuan, B. Zhang, and X.-J. Bi, *Phys. Rev. D* **84**, 0905.0105.

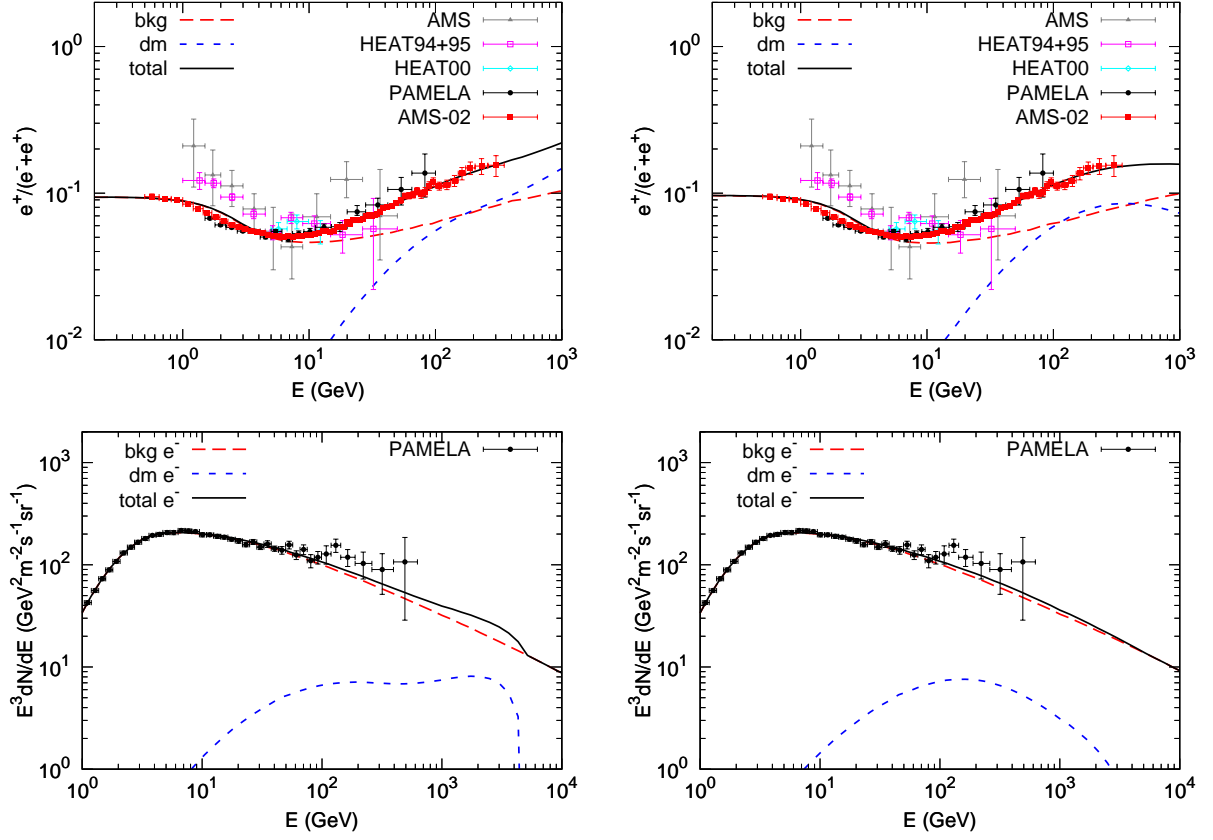


FIG. 12: The positron fraction (top) and electron spectrum (bottom) for the best fitting parameters of the fit II-a with DM annihilation into  $W^+W^-$  (left) and  $b\bar{b}$  (right) channels.

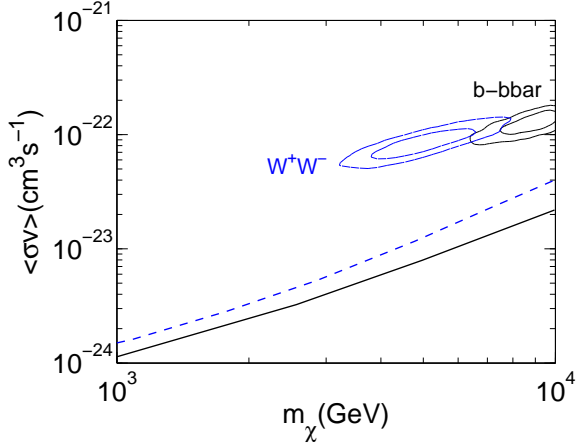


FIG. 13:  $1\sigma$  and  $2\sigma$  confidence regions on the DM mass and cross section plane derived from fit II-a, for  $W^+W^-$  and  $b\bar{b}$  channels. The lines show the upper limits derived using Fermi four year observations on the dwarf galaxies for  $W^+W^-$  (dashed) and  $b\bar{b}$  (solid) channels [60].

043002 (2011), 1104.3357.

[54] J. Alcaraz, et al., Phys. Lett. B **490**, 27 (2000).

[55] T. Sanuki, et al., Astrophys. J. **545**, 1135 (2000),

arXiv:astro-ph/0002481.

- [56] M. Aguilar, et al., Phys. Lett. B **646**, 145 (2007), arXiv:astro-ph/0703154.
- [57] S. W. Barwick, et al., Astrophys. J. Lett. **482**, L191 (1997), arXiv:astro-ph/9703192.
- [58] S. Coutu, et al., in *International Cosmic Ray Conference* (2001), vol. 5 of *International Cosmic Ray Conference*, p. 1687.
- [59] X. Huang, Q. Yuan, P.-F. Yin, X.-J. Bi, and X. Chen, J. Cosmol. Astropart. Phys. **11**, 048 (2012), 1208.0267.
- [60] A. Drlica-Wagner, in *Fermi Symposium 2012* (2012).
- [61] M. Boezio, et al., Astrophys. J. **532**, 653 (2000).
- [62] M. Ackermann, et al., Physical Review Letters **107**, 241302 (2011), 1108.3546.
- [63] A. Geringer-Sameth and S. M. Koushiappas, Physical Review Letters **107**, 241303 (2011), 1108.2914.
- [64] T. Delahaye, R. Lineros, F. Donato, N. Fornengo, J. Lavalle, P. Salati, and R. Taillet, Astron. Astrophys. **501**, 821 (2009), 0809.5268.
- [65] G. D. Badhwar, R. L. Golden, and S. A. Stephens, Phys. Rev. D **15**, 820 (1977).
- [66] L. Feng, R.-Z. Yang, H.-N. He, T.-K. Dong, Y.-Z. Fan, and J. Chang, ArXiv e-prints (2013), 1303.0530.
- [67] M. Papucci and A. Strumia, J. Cosmol. Astropart. Phys. **3**, 14 (2010), 0912.0742.
- [68] M. Cirelli, P. Panci, and P. D. Serpico, Nuclear Physics B **840**, 284 (2010), 0912.0663.